Applied Mathematical Modelling 92 (2021) 669–686

Contents lists available at ScienceDirect

Applied Mathematical Modelling

journal homepage: www.elsevier.com/locate/apm

Controlling the natural convection of a non-Newtonian fluid using a flexible fin

Mohammad Shahabadi[a], S.A.M. Mehryan[b], Mohammad Ghalambaz[c,d,*], Muneer Ismael[e]

[a] Department of Mechanical Engineering, Isfahan University of Technology, Isfahan, Iran
[b] Young Researchers and Elite Club, Yasooj Branch, Islamic Azad University, Yasooj, Iran
[c] Metamaterials for Mechanical, Biomechanical and Multiphysical Applications Research Group, Ton Duc Thang University, Ho Chi Minh City, Vietnam
[d] Faculty of Applied Sciences, Ton Duc Thang University, Ho Chi Minh City, Vietnam
[e] Mechanical Engineering Department, College of Engineering, University of Basrah, Basrah, Iraq

ARTICLE INFO

Article history:
Received 25 February 2020
Revised 19 September 2020
Accepted 15 November 2020
Available online 24 November 2020

Keywords:
Flexible fin
Fluid-Structure Interaction (FSI)
Moving mesh
Non-Newtonian natural convection

ABSTRACT

In the present study, the flow and heat transfer of a power-law non-Newtonian fluid in a cavity are addressed. The top and bottom walls of the cavity are well insulated, the left vertical wall is at a hot temperature, and the right wall is at a low temperature. A flexible elastic fin is mounted at the hot wall of the cavity. The non-Newtonian fluid circulates inside the cavity due to the buoyancy forces. Fluid-Structure Interaction (FSI) and the non-Newtonian flow within the cavity and the hot fin are coupled. The flow interaction with the fin leads to the deformation of the fin, and the change in the shape of the fin changes the flow and heat transfer. Hence, the coupling between the fluid and the structure is two ways. The Arbitrary Lagrangian-Eulerian (ALE) along the moving mesh method is employed to model the deflection of the structure inside the fluid domain. The finite element method is adopted to solve the governing equations. The results show that the deflection of the fin is higher for a dilatant non-Newtonian fluid, compared to the pseudoplastic and Newtonian fluids. The number of flow vortexes and flow hydrodynamic notably change by the variation non-Newtonian index. The variation of the non-Newtonian index produce minimal effects on the heat transfer rate. Moving from pseudoplastic effects to Newtonian and dilatant effects reduces the heat transfer rate and increases the internal stresses in the fin. Moreover, the maximum stress in stiff-fins is higher than soft-fins.

1. Introduction

Convective heat transfer between a solid surface and the surrounding fluid can occur due to the difference in fluid densities caused by local heating in the presence of gravity field (natural convection) and (or) under the effect of external forces (forced convection). In cavities, the former mechanism may be sorted as passive heat transfer, while the later one is sorted as efficient heat transfer. Nevertheless, the natural convection mechanism can be promoted by keeping its passive nature. One of the strategies followed in promoting natural convection is the generation of perfect mixing among fluid particles

* Corresponding author at: Ton Duc Thang University, Ho Chi Minh City, Vietnam.
E-mail address: mohammad.ghalambaz@tdtu.edu.vn (M. Ghalambaz).

https://doi.org/10.1016/j.apm.2020.11.029
0307-904X/

Nomenclature

$\boldsymbol{d}_s$	displacement vector;
E	dimensional Young's modulus;
E_τ	non-dimensional elasticity modulus;
f	frequency;
$\boldsymbol{F}_v$	vector of volume force;
$\boldsymbol{g}$	gravity vector;
L	characteristic size (enclosure high and width);
P	pressure filed;
Pr	Prandtl number;
Ra	Rayleigh number;
t	time in dimensional form;
T	temperature field;
$\boldsymbol{u}$	velocity vector;
$\boldsymbol{w}$	the moving mesh velocity vector;
x, y	Cartesian coordinates

Greek symbols

α	coefficient of the thermal diffusivity
β	coefficient of the volumetric thermal expansion
σ	field of the tensor of stress
τ	dimensionless time
μ	the fluid's dynamic viscosity
ν	Poisson's ratio
ρ	density
ρ_R	the ratio of fluid to solid-structure density

Subscripts

avg	the average property
c	the cold wall
f	the fluid property
h	the hot property
s	the flexible plate

Superscripts

tr	matrix transpose
*	dimensional for of variables and parameters

using baffles or supplementing the heat transfer unit with a mean of thinning or breaking down the thermal boundary layers like obstacles and ribs [1]. Some aspects of natural convection heat transfer, such as entropy generation [2,3], hydromagnetic effects [4,5], double-diffusive convection heat transfer [6], nanofluids [3,7], conjugate heat transfer [8], and porous cavities [9] have been addressed in recently published papers. Flexible segments are thin strips made from materials having low elasticity modulus, which can be considered as a new aspect of heat transfer control in natural convection flows in enclosures.

When these strips are fixed from one end, they are known as "fin", and when its two ends are fixed, they are known as "insert". These strips deform when exposed to hydrodynamic forces, thereby altering the domain of fluid flow and influencing the thickness of the adjacent boundary layer and also forming new circulation behaviors. In addition to these features, flexible strips are accompanying with lower pressure drop [10]. Ghalambaz et al. [11] supposed a sine wave excited flexible fin mounted to a vertical hot wall of a square cavity and inspected the impact of its length and the amplitude of the excitation. They used the Fluid-Structure Interaction (FSI) approach in a moving mesh domain. Their conclusions showed that flexible fin exhibits higher Nusselt number than a rigid fin, but lengthening it produces adverse action on Nusselt number. They also concluded that the higher the amplitude of oscillation is the higher the values of Nusselt number. Also, the mixed convection heat transfer effect of two conciliating fins was investigated in [12], and it was found that the flexibility of the fins could enhance the heat transfer.

Ismael and Jasim [13] suggested the utilization of a free end flexible fin in controlling the thermal boundary layer formed along a hot wall of a vented cavity. They fixed the other end of the fin on a horizontal wall such that it faces the input port and next to the hot wall. Around 230% increase in the average Nusselt number was reported in case of using a flexible fin compared with no fin. The distance of the fin position from the inlet port was also significant. Raisi and Arvin [14] went farther with the FSI problem, where they considered a square cavity with a flexible top wall. In addition, they included a

flexible horizontal baffle with two fixed ends positioned transversely in the middle of the cavity. They deduced that the deformations in both the wall and the baffle exhibit storage energy. The storage energy then discharged to interact with fluid leading to strengthening the circulation and hence augmenting the exchange of thermal energy.

The FSI approach has been revisited by Kuttler and Wall [15] to introduce a simple and robust solver for FSI problems. One of their applications was a square cavity with a flexible bottom-wall and a moving lead, which later was adopted as a benchmark case for validation of FSI codes. Thereby, studies regarding different cavities with flexible-walls have been proclaimed in the literature [16,17]. Most of these studies endorse a notable role of the deformed flexible wall on the streamlines and heat transfer characteristics. Flexible wall splitting a cavity vertically and diagonally were also studied extensively in the scope of natural convection like an piezoelectric excitation [18], external flow [19], 3D cavity with bottom flexible wall [20], and a particulated flow [21]. These studies demonstrated that the deformation in the splitter resulted in a notable change of Nusselt number owing to the expanding and shrinking of the sub-cavities.

In many practical applications, the viscosity of the working fluid may not be held constant with the gradient of velocity (shear rate), i.e., the relation between the shear stress and shear rate is non-linear. These fluids, which are known as non-Newtonian, are found in a long list of applications like fluid used in the drilling process (drilling mud), molten polymers, paints, thermoplastics, and biological applications [22]. Cooling systems of electronics, compact heat exchangers [23], and cementing walls, including cavities, are other practical examples. The importance of the non-Newtonian fluids in convective heat transport systems arises from the violent variations in viscous forces.

Owing to the wider literature, the work of Acrivos et al. [24] is sorted as one of the pillars in the heat transfer and the boundary layer aspect of non-Newtonian fluids over different solid cylinders. Dhiman [25] investigated the flow and heat transfer of dilatant fluids in the forced convection of a channel containing a square shape cylinder. It was found that the Nusselt number along a heated square cylinder exposed to a power-law flow-flow is higher for a case of constant heat flux compared to a case of constant wall temperature. Cavadas et al. [26] carried out experimental investigation supported by numerical simulation about Newtonian and non-Newtonian fluids emanating from a rectangular slot and impinging on a flat plate. They reported that a jet of a non-Newtonian polymer solution is stronger than a jet of a Newtonian fluid.

Although there are many published works regarding forced convection of non-Newtonian fluids in channels, we will focus on natural convection aspects in a cavity to complying with the aim of the present work. The denominated study of Ozoe and Churchill [27] is considered as the first work regarding the convection of non-Newtonian fluids in enclosures. They focused on the stability aspects of two types of shear-thinning (power-law) fluids in a shallow enclosure heated from below and cooled from the top, i.e., Rayleigh-Benard problem. It was found that the onset of the instability aspect delays with increasing the power index of both models.

Ohta et al. [28] inspected the natural convection in a square cavity filled with a shear-thinning fluid and found that the transient recirculation concomitant the non-Newtonian fluids is more complicated than those of Newtonian fluid. Khezzar et al. [29] showed that for an inclined rectangular cavity, the flow structures manifest opposite evolutions with a power-law index of shear-thinning and thickening fluids. It was found that the flow becomes more stable for high Prandtl number and shear-thickening fluids. Matin et al. [23] simulated the convective flow of power-law (Ostwald–de Waele) fluids between two eccentric annuli by natural convection in an enclosure including a heated square obstacle. It was shown that the Nusselt number decreases with increasing the power-law index. The position of the obstacle and the aspect ratio were affected by the heat transfer process significantly.

Alloui and Vasseur [30] showed that for a low Rayleigh number in a vertical enclosure, the Carreau–Yasuda (yield-pseudoplastic) model predicts similar Nusselt numbers compared with the power-law model. Nevertheless, for intermediate Rayleigh numbers, it was found that the Nusselt number estimated by Carreau–Yasuda is higher than that estimated by the power-law model. Selimefendigil and Chamkha [31] applied an inclined magnetic field upon a cavity filled with power-law fluid. This fluid is subjected to shear effect at the upper moving wall while it is heated from a corrugated bottom wall. Similar results were mentioned that is the Nusselt number of shear-thinning fluids is greater than shear-thickening and Newtonian fluids. The retardation effect of the magnetic field was observed in all Newtonian and non-Newtonian fluids. It can be asserted, consequently, that the shear-thinning fluids are axiomatically produce higher Nusselt number due to the reduction of viscous forces. Alsabery et al. [32] also demonstrated this axiomatic when presented results of natural convection in a trapezoidal cavity of sinusoidal heating and cooling and filled with power-law fluids with nanoparticles dispersed. Even when the power-law fluid is saturated with porous medium confined in an open-sided cavity, the Nusselt number is higher for shear-thinning fluids, as presented by Raizah et al. [33].

Regarding the FSI topic and the case of non-Newtonian fluids, our best survey has shown no published works esteeming the heat exchange and flow aspects of non-Newtonian FSI in cavities. However, there are only some scarce works focusing on the forced convection hydrodynamics aspect of non-Newtonian fluids with flexible wall channels as in Anand et al. [34] and Qiao et al. [35]. As such, the present study aims to address the natural convection flow and heat transfer in a cavity containing a non-Newtonian fluid interacting with a flexible thin fin for the first time.

2. Modeling approach

The geometry of interest in the current work, which is illustrated in Fig. 1, is a cavity with a flexible fin attached to the hot left wall. The square cavity having the size of L^* is filled by a power-law non-Newtonian fluid. The buoyancy force, resulting from the natural convection causes the flexible fin to bend. The temperature of the left and right walls are consid-

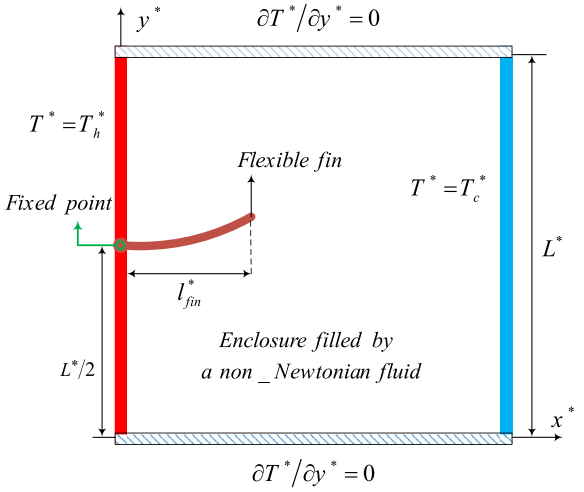

Fig. 1. A schematic of the physical model; 2D enclosure filled by a non-Newtonian fluid and a flexible fin attached to its hot wall.

ered T_h^* and T_c^*, whereas the upper and lower walls are insulated thermally. The no-slip condition is considered for all the walls, including the outer walls of the cavity and the surfaces of the fin. The flexible fin of thickness t_{fin}^* is considered to be isotropic and uniform. The temperature differences were assumed limited. Hence, the thermophysical properties were considered independent of temperature, except for the density variation of the liquid, which was taken into account by using the Boussinesq model.

Utilizing the assumptions mentioned earlier and employing the Arbitrary Lagrangian-Eulerian (ALE) technique, the equations modeling the hydrodynamic and thermal characteristics of the problem are presented as follows [14,36]:

Continuity equation:

$$\nabla^* \cdot \mathbf{u}^* = 0 \tag{1}$$

Momentum equations:

$$\rho_f \left[\frac{\partial \mathbf{u}^*}{\partial t} + (\mathbf{u}^* - \mathbf{w}^*) \cdot \nabla^* \mathbf{u}^* \right] - \nabla^* \cdot \left[-P^* I + \mu \left(\nabla^* \mathbf{u}^* + (\nabla^* \mathbf{u}^*)^{tr} \right) \right] - \rho_f \beta \mathbf{g} (T^* - T_c^*) = 0 \tag{2}$$

In which

$$\mu(\dot{\gamma}) = m\mu_a \begin{vmatrix} \mu_a = (\dot{\gamma})^{n-1} \\ \dot{\gamma} = \max\left(\sqrt{[\mathbf{D}^*] : [\mathbf{D}^*]}, \dot{\gamma}_{\min} \right) \\ 2\mathbf{D}^* = \nabla \mathbf{u}^* + (\nabla \mathbf{u}^*)^{tr} \end{vmatrix} \tag{3}$$

As well-known, the change of the apparent viscosity by the variation of the shear-rates is linear for Newtonian fluids. However, a non-linear relation between the apparent-viscosity and shear-rate can lead to non-Newtonian behaviors. The non-Newtonian fluids can be dilatant ($n > 1$) or pseudoplastic ($n < 1$). A fluid with $n = 1$ is known as a Newtonian fluid. The apparent-viscosity elevates with the growth of shear-rate for dilatant fluids. In contrast, the apparent-viscosity decays by the growth of shear rates when the fluid is pseudoplastic.

The energy equation for the fluid:

$$(\rho c_p)_f \left[\frac{\partial T^*}{\partial t} + (\mathbf{u}^* - \mathbf{w}^*) \cdot \nabla^* T^* \right] - k_f \nabla^{*^2} T^* = 0 \tag{4}$$

The energy equation for the flexible fin:

$$(\rho c_p)_s \frac{\partial T^*}{\partial t} - k_s \nabla^{*^2} T^* = 0 \tag{5}$$

Furthermore, the motion of flexible fin is described using the nonlinear elastodynamic equation mentioned below:

$$\rho_s \frac{d^2 \mathbf{d}_s^*}{dt^2} - \nabla^* \boldsymbol{\sigma}^* = \mathbf{F}_v^* \tag{6}$$

where, $\mathbf{u^*} = (u^*, v^*)$ represents velocity vector of the fluid, $\mathbf{w^*} = (u_s^*, v_s^*)$ shows the velocity of moving coordinate system, P^* and T^* as the pressure of the fluid and temperature of the solid/ fluid, respectively, $\mathbf{g}$ the gravity acceleration. $\boldsymbol{\sigma^*}$ shows the solid stress tensor, $\mathbf{d}_s^*$ denotes the displacement vector of the fin so that $d\mathbf{d}_s^*/dt = \mathbf{w^*}$, and $\mathbf{F}_v^*$ indicates the body

force imposed on the flexible fin. ρ represents the density (f and s subscripts refer to the fluid and solid, respectively). α_f is thermal diffusivity of the fluid, α_s thermal diffusivity of the solid, ν_f is the kinematic viscosity, and β shows the volumetric thermal expansion coefficient of the fluid. The Neo-Hookean solid model is applied to express the stress tensor of Eq. (6).

$$\boldsymbol{\sigma}^* = J^{-1}FSF^{tr}\Big|F = \left(I + \nabla^*\mathbf{d}_s^*\right), J = det(F)\,\&\,S = \partial W_s/\partial\varepsilon \tag{7-a}$$

$$W_s = \frac{1}{2}\ell\left(J^{-1}I_1 - 3\right) - \ell\ln(J) + \frac{1}{2}\lambda(\ln(J))^2\Bigg|\begin{matrix}\ell = E/(2(1+\nu))\\ \lambda = E\nu/((1+\nu)(1-2\nu))\end{matrix} \tag{7-b}$$

$$\varepsilon = \frac{1}{2}\left(\nabla^*\mathbf{d}_s^* + \nabla^*\mathbf{d}_s^{*tr} + \nabla^*\mathbf{d}_s^{*tr}\nabla^*\mathbf{d}_s^*\right) \tag{7-c}$$

The boundary conditions applied to the outer walls and the interface of the flexible fin and non-Newtonian fluid can be written as: at the hot wall:

$$T^* = T_h^*, u^* = v^* = 0 \tag{8-a}$$

at the cold wall:

$$T^* = T_c^*, u^* = v^* = 0 \tag{8-b}$$

At the upper and lower walls:

$$\partial T^*/\partial y^* = 0, u^* = v^* = 0 \tag{8-c}$$

at the interface of the flexible fin and non-Newtonian fluid:

$$k_f\frac{\partial T}{\partial n}|_f = k_s\frac{\partial T}{\partial n}|_s,\ \frac{\partial\mathbf{d}_s^*}{\partial t} = \mathbf{u}^*,\ \left[-P^*I + \mu(\dot{\gamma})\left(\nabla^*\mathbf{u}^* + (\nabla^*\mathbf{u}^*)^{tr}\right)\right]\cdot n - \boldsymbol{\sigma}^*\cdot n = 0 \tag{8-d}$$

The transition to the non-dimensional coordinates can be done using the following variables:

$$\begin{aligned}&(x, y, t_{fin}) = \frac{(x^*, y^*, t_{fin}^*)}{L^*}, \mathbf{d}_s = \frac{\mathbf{d}_s^*}{L^*}, \nabla^* = L^*\nabla, \boldsymbol{\sigma} = \frac{\boldsymbol{\sigma}^*}{E}\\ &\mathbf{u} = \frac{\mathbf{u}^*L^*}{\alpha_f}, \mathbf{w} = \frac{\mathbf{w}^*L^*}{\alpha_f}, P = \frac{P^*L^{*2}}{\rho_f\alpha_f^2}, \tau = \frac{t\alpha_f}{L^{*2}}, T = \frac{T^* - T_c^*}{T_h^* - T_c^*}\end{aligned} \tag{9}$$

In the dimensionless form, the equations are written as follows:

$$\nabla\cdot\mathbf{u} = 0 \tag{10}$$

$$\frac{\partial\mathbf{u}}{\partial\tau} + (\mathbf{u} - \mathbf{w})\cdot\nabla\mathbf{u} + \nabla\cdot\left[-PI + Pr\dot{G}^{n-1}(\nabla\mathbf{u} + (\nabla\mathbf{u})^{tr}\right] - PrRaT\mathbf{j} = 0 \tag{11}$$

where

$$\dot{G} = max\left(\sqrt{[\mathbf{D}]:[\mathbf{D}]}, \dot{G}_{min}\right)|2\mathbf{D} = \nabla\mathbf{u} + (\nabla\mathbf{u})^{tr} \tag{12}$$

Also, the Rayleigh and Prandtl numbers are introduced as:

$$Ra = \frac{\rho_f g\beta_f\left(T_h^* - T_c^*\right)L^{2n+1}}{m_f\alpha_f^n}, Pr = \frac{m_f}{\rho_f\alpha_f}\left(\frac{\alpha_f}{L^2}\right)^{n-1} = \frac{m_f}{\rho_f}\frac{\alpha_f^{n-2}}{L^{2n-2}} \tag{13}$$

$$\frac{\partial T}{\partial\tau} + (\mathbf{u} - \mathbf{w})\cdot\nabla T = \nabla^2 T \tag{14}$$

$$\rho_r c_{p,r}\frac{\partial T}{\partial\tau} = k_r\nabla^2 T \tag{15}$$

$$\rho_r\frac{d^2\mathbf{d}_s}{d\tau^2} - E_\tau\nabla\boldsymbol{\sigma} = E_\tau\mathbf{F}_v \tag{16}$$

where

$$E_\tau = \frac{EL^{*2}}{\rho_f\alpha_f^2}, \mathbf{F}_v = \frac{\left(\rho_f - \rho_s\right)L^*\mathbf{g}}{E}, \rho_r = \frac{\rho_s}{\rho_f}, k_r = \frac{k_s}{k_f}, c_{p,r} = \frac{c_{p,s}}{c_{p,f}} \tag{17}$$

The dimensionless boundary conditions are:
At the hot wall:

$$T = 1, u = v = 0 \tag{18-a}$$

At the cold wall:

$$T = 0, u = v = 0 \tag{18-b}$$

At the upper and lower walls of the cavity:

$$\partial T/\partial y = 0, u = v = 0 \tag{18-c}$$

At the interface of the flexible fin and non-Newtonian fluid:

$$\left(\frac{\partial \theta_f}{\partial n}\right) = \kappa\left(\frac{\partial \theta_s}{\partial n}\right), \frac{\partial \mathbf{d}_s}{\partial \tau} = \mathbf{u}, \left[-PI + Pr\dot{G}^{n-1}\left(\nabla \mathbf{u} + (\nabla \mathbf{u})^{tr}\right)\right] \cdot n - E_\tau \boldsymbol{\sigma} \cdot n = 0 \tag{18-d}$$

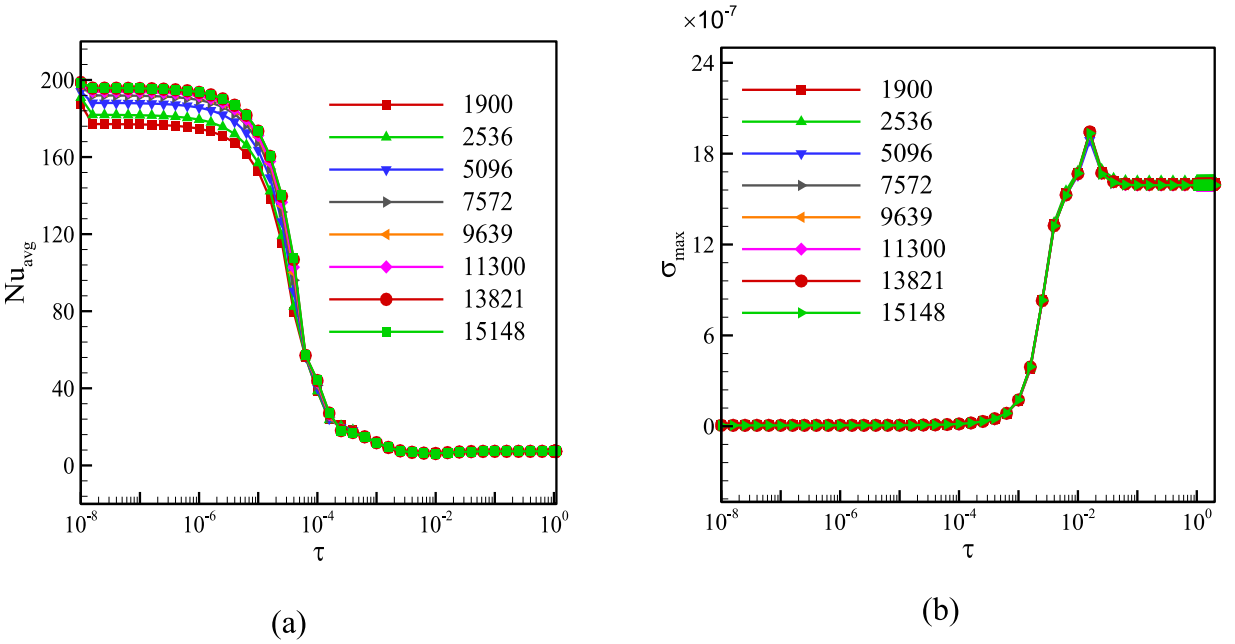

Fig. 2. The variations of (a): Nusselt number on the hot wall and (b): the maximum values of stress on the fin for different meshes at $n = 0.8$, $Ra = 10^5$, $Pr = 10$, $E_\tau = 10^{10}$.

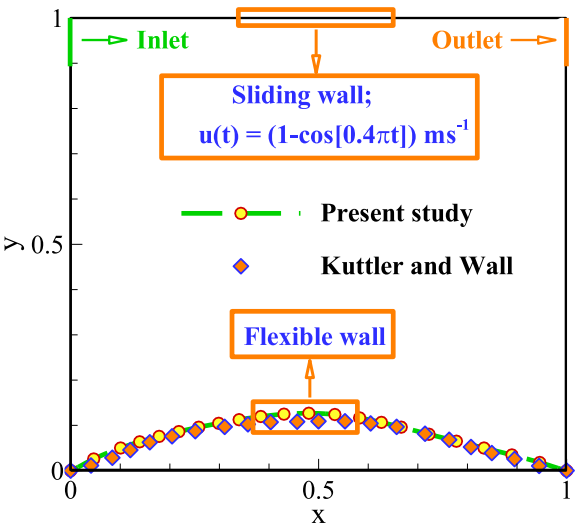

Fig. 3. The comparison between the results of this study and Kuttler and Wall's [15]; $\rho_f = 1$ kg/m^3, $\upsilon_f = 0.001$m^2/s, $\rho_s = 500$ kg/m^3, $E = 250$ N/m^2.

In non-dimensional spaces, the initial pressure and velocity of the fluid are considered zero. Furthermore, the initial temperature is 0.5. The maximum velocity corresponds to the maximum Rayleigh number of 10^5. In this case, the non-dimensional velocity value was computed as $u = 384$ or $O(10^{+2})$. By using a typical value of thermal diffusivity of α in the order $O(10^{-7})$ m^2/s and a cavity with a minimum size of L^*~$O(10^{-2})$ m, the maximum dimensional velocity in the cavity was computed as $O(u^*)$~$O(u) \times O(\alpha)/O(L^*)$~$O(10^{-3})$ m/s. It is clear that this maximum velocity value for a larger cavity will be even lower. Using this velocity and taking into account a temperature difference of $\Delta T = T_h^* - T_c^*$~$O(10^{+1})$ °C and a specific heat capacity of $O(10+^3)$ J/(kg.K), the Eckert number was computed as $O(Ec)$~$O(u^{*2})/(O(c_p) \times O(\Delta T))$~$10^{-6}/(10^{+3} \times 10^{+1})$~$10^{-2}$. As seen, the order of Eckert number is about 0.01. The order of the Brinkman number ($Pr \times Ec$) was also computed as $O(Pr) \times O(Ec)$~$10^{+1} \times 10^{-2}$~0.1. It should be noted that these values were obtained for the maximum fluid velocity, while in most parts of the enclosure, the fluid's velocities are minimal and zero at the walls. Hence, due to small values of Eckert and Brinkman numbers, the viscous dissipation terms compared to heat transfer terms were neglected in the present study.

The non-dimensionless heat transfer rates through the fluid adjacent to the hot wall and the fin basis are, respectively:

$$Nu_f = -\frac{\partial \theta}{\partial X} \tag{19-a}$$

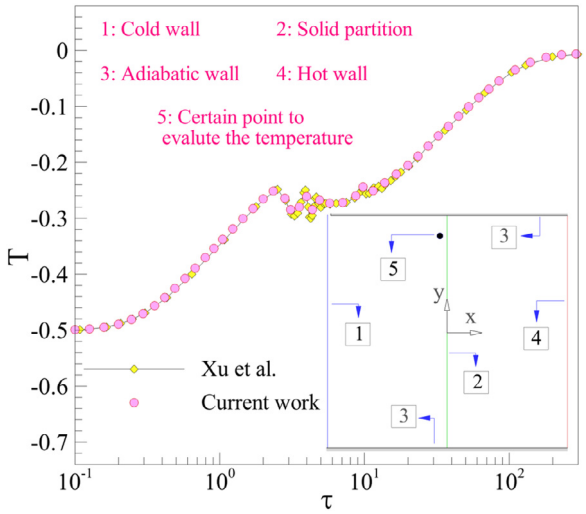

Fig. 4. The comparison between the temperature of a certain point within the cavity of this study and Xu et al. [39] at $Pr = 6.63$ and $Ra = 9.2 \times 10^8$.

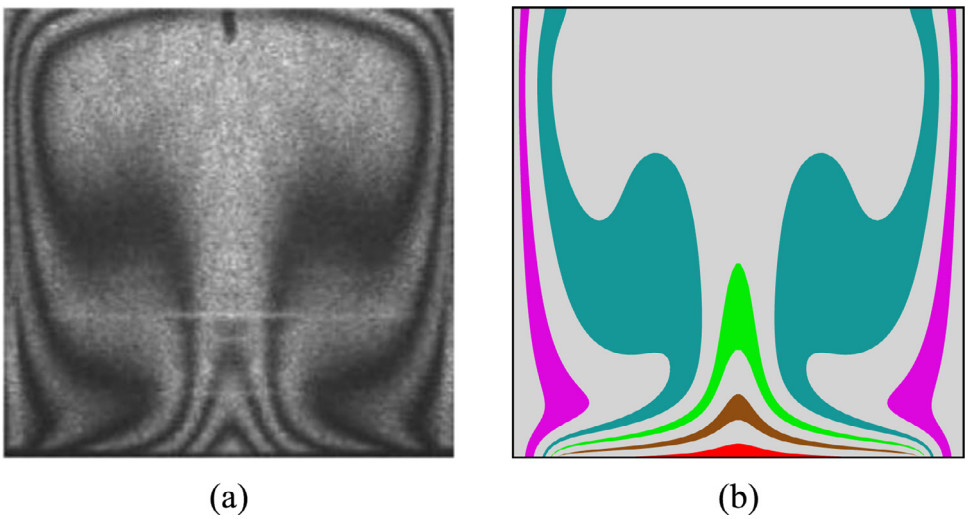

Fig. 5. a): The temperature field of experimental studies by Calcagni et al. [40] and b): The temperature field of numerical studies of the present study at $Pr = 0.71$ and $Ra = 1.836 \times 10^5$.

$$Nu_s = -k_r \frac{\partial \theta}{\partial X} \tag{19-b}$$

The average Nusselt number at the wall is also introduced as:

$$\overline{Nu} = \int_0^{s_1} Nu_f dy + \int_{s_1}^{s_2} Nu_s dy + \int_{s_2}^{1} Nu_f dy \Big| \begin{matrix} s_1 = \frac{1}{2} - \frac{t_{fin}}{2} \\ s_2 = \frac{1}{2} + \frac{t_{fin}}{2} \end{matrix} \tag{20}$$

Ultimately, the following partial differential equation is solved to visualize the flow patterns of the fluid:

$$\nabla^2 \psi = -\nabla \times \mathbf{u} \tag{21}$$

The value of ψ, namely stream function, on the outer walls of the enclosure, is zero.

3. The numerical method, grid study, and verification

3.1. Numerical approach and mesh independency

The Galerkin finite element method (FEM), with the aid of the ALE technique, is applied to solve the interdependent, complex, and non-linear governing equations. Some aspect of the numerical approach of the finite element is expressed in [37,38]. In this work, the Gaussian quadrature, based on the FEM, provides smooth solutions at the internal sub-domains. We have treated the finite viscosity in the limit of zero shear rates by defining a lower limit of the shear rate to be 0.01 s^{-1}. Triangular non-uniform elements have been used for the mesh generation of studied fluid domains. However, for the fin, the mapped elements have been utilized. The fully coupled approach was employed to couple the heat, momentum, structure, and mesh displacements. Hence, a large matrix of coefficients was constructed, which was solved by the Newton method at each time step.

To achieve accurate results in numerical simulations, mesh independency study is one of the most critical steps. According to Fig. 2, the average Nusselt number on the hot wall, and the maximum values of stress on the fin have been determined for different mesh numbers. Mesh study has been performed in such a way that meshes are refined until the variation of the average Nusselt number and maximum stress on the fin are negligible. It can be seen that the difference between the obtained results of the mesh with 13821 and 15148 elements is insignificant. Thus, the mesh with 13821 elements has been chosen for numerical studies to reduce the computational cost with acceptable accuracy. It is worth noting that there were overall 45 elements on both the thickness and length of the flexible fin. The dimensionless length and width of fin were divided into 12 and 3 sections, respectively.

3.2. Comparisons with others

The accuracy and correctness of the obtained results must be validated through other numerical and experimental investigations. First, the outcomes of the investigation of Kuttler and Wall [15] have been used for the validation of this study.

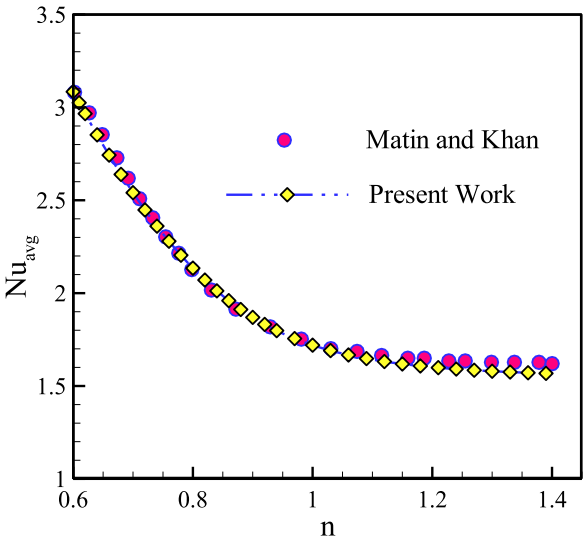

Fig. 6. Average Nusselt number for various values of the power-law index (n): the present work (dash-dot line), and the outcomes of Matin and Khan [41] (points) at $Pr = 10$ and $Ra = 10^3$.

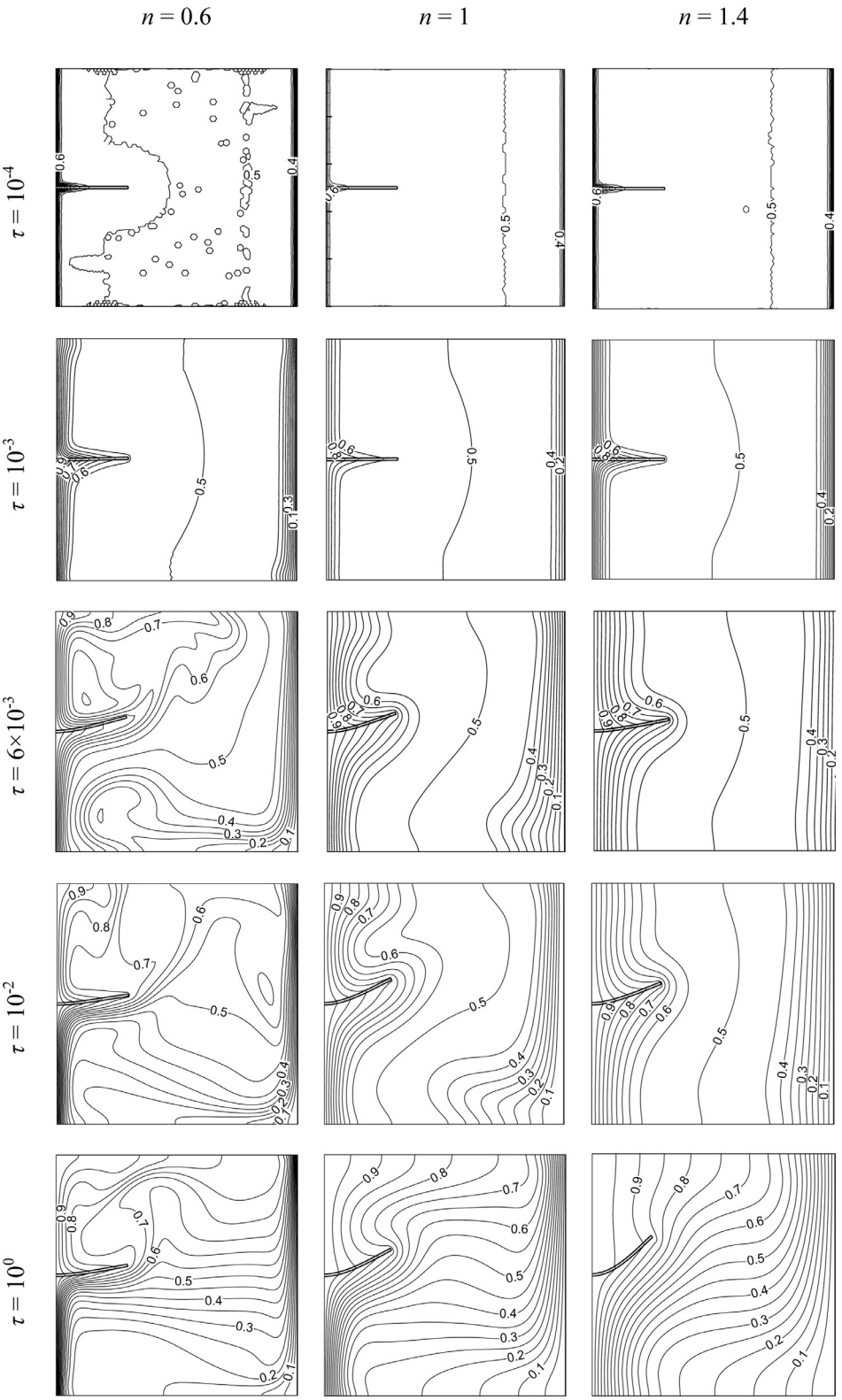

Fig. 7. Time variation of isotherms at $Ra = 10^5$, $Pr = 10$, and $E_\tau = 10^{10}$.

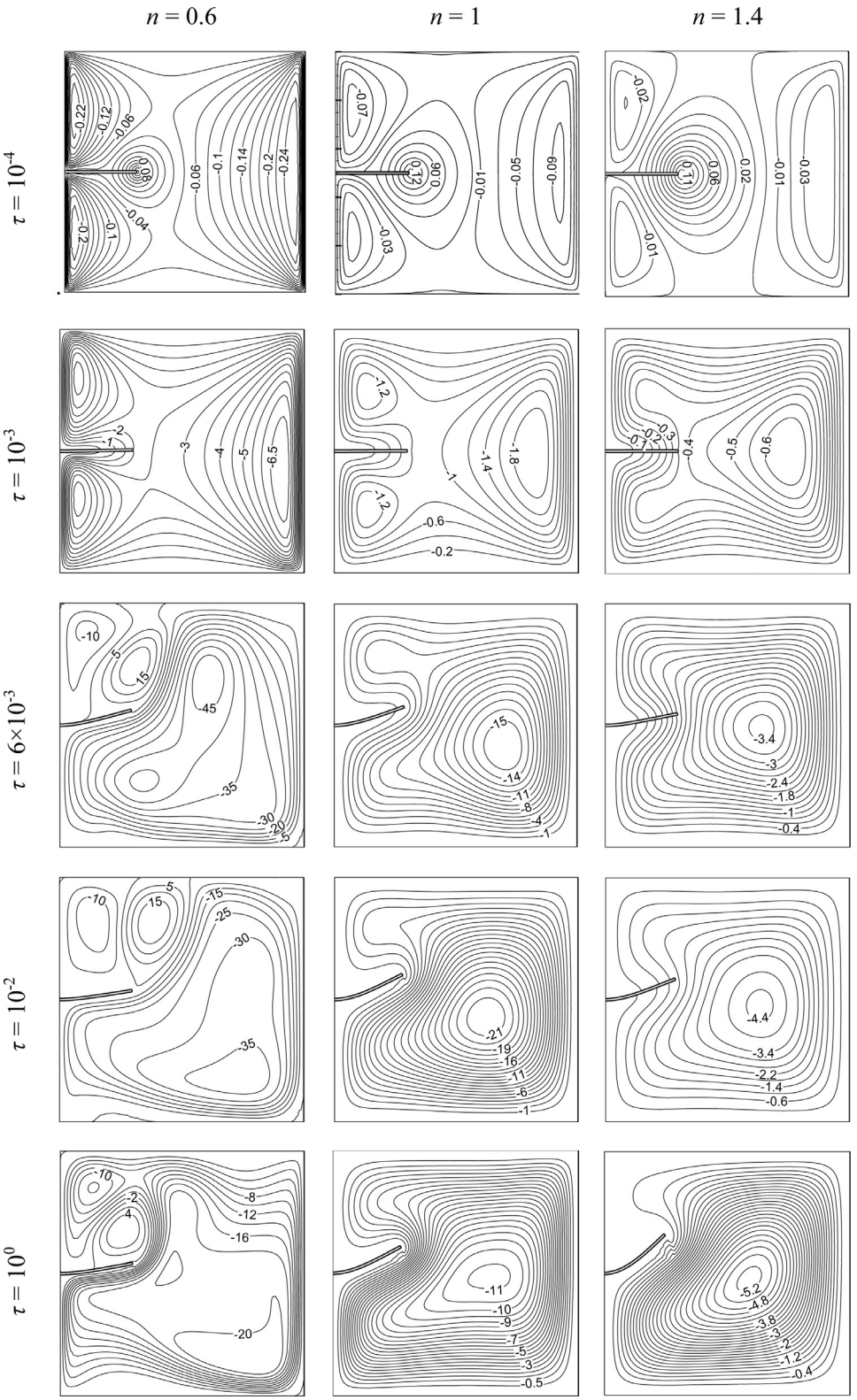

Fig. 8. Time variation of streamlines at $Ra = 10^5$, $Pr = 10$, and $E_\tau = 10^{10}$.

They examined the lid-driven cavity equipped with a deformable bottom wall. The flexible bottom wall is deformed by the fluid and solid interaction induced by the created vortexes due to the upper wall displacement. As depicted in Fig. 3, the comparison between the results of this study and Kuttler and Wall's for the displacement of the flexible wall shows a good agreement.

Second, the temperature of a certain point within the cavity of this study and Xu et al. [39] is compared at different time snaps. The location of the mentioned point for extracting the local temperature is at (−0.0083,0.375), shown in Fig. 4. The horizontal walls of the cavity were adiabatic, while the left and right vertical walls of the cavity were kept at low and high temperatures, respectively. As seen in Fig. 4, the obtained local temperature of the designated point of this study and [39] shows a desirable agreement.

Third, to validate the natural convection behavior within the cavity, the results of this study are compared with the experimental investigations of Calcagni et al. [40]. An identical temperature field can be seen for both studies [40], verifying the excellent agreement of the results.

Finally, for validation of the natural convection mechanism of a non-Newtonian power-law fluid within a cavity, the Matin and Khan [41] numerical modeling has been re-simulated by the code employed in the current study. These authors addressed the free convection flow and heat transfer mechanism of a non-Newtonian power-law fluid in a rigid cavity enclosure. The enclosure was the annuli of the horizontal cylinders where the inner cylinder was hot, and the outer cylinder was cold. Fig. 6 demonstrates an excellent agreement between average Nusselt numbers of the current work and those of [41] for a non-Newtonian fluid when $Ra = 10^3$, $Pr = 10$, and various values of n (power-law index).

4. Results and discussion

The effects of different parameters on the thermo-flow fields and the deformation of the flexible fin are studied in this section. The variable parameters are the elasticity modulus ($5 \times 10^9 \leq E_\tau \leq 10^{11}$), Rayleigh number ($10^3 \leq Ra \leq 10^5$) and power-law index ($0.6 \leq n \leq 1.4$), while the other important parameters like the dimensionless body force ($F_v = 0$), the plate's thickness ($t_{fin} = 0.01$), thermal conductivity ratio ($k_r = 100$), Prandtl number ($Pr = 10$), and density ratio ($\rho_R = 1$) are considered constant during the numerical simulations.

Figs. 7 and 8 depict the transient progression of isotherms and streamlines for non-Newtonian power-law fluid with different values of n at $Ra = 10^5$, $Pr = 10$, $E_\tau = 10^{10}$. According to Fig. 7, at initial time snaps ($\tau = 10^{-4}$ and 10^{-3}), the conduction heat transfer is the main mechanism, and the fluid occupies most of the cavity at the initially given temperature. As time passes, more disturbance can be seen around the fin, and isotherms move toward it, so the convection mechanism becomes significant compared with the conduction mechanism. At the steady-state ($\tau = 10^{\circ}$), horizontal and vertical stratification of isotherms can be seen for $n = 0.6$ and $n = 1.4$, respectively. The vertical pattern of $n = 1.4$ is the result of the resistance of the dilatant non-Newtonian fluid against the buoyancy force produced by convective heat transfer.

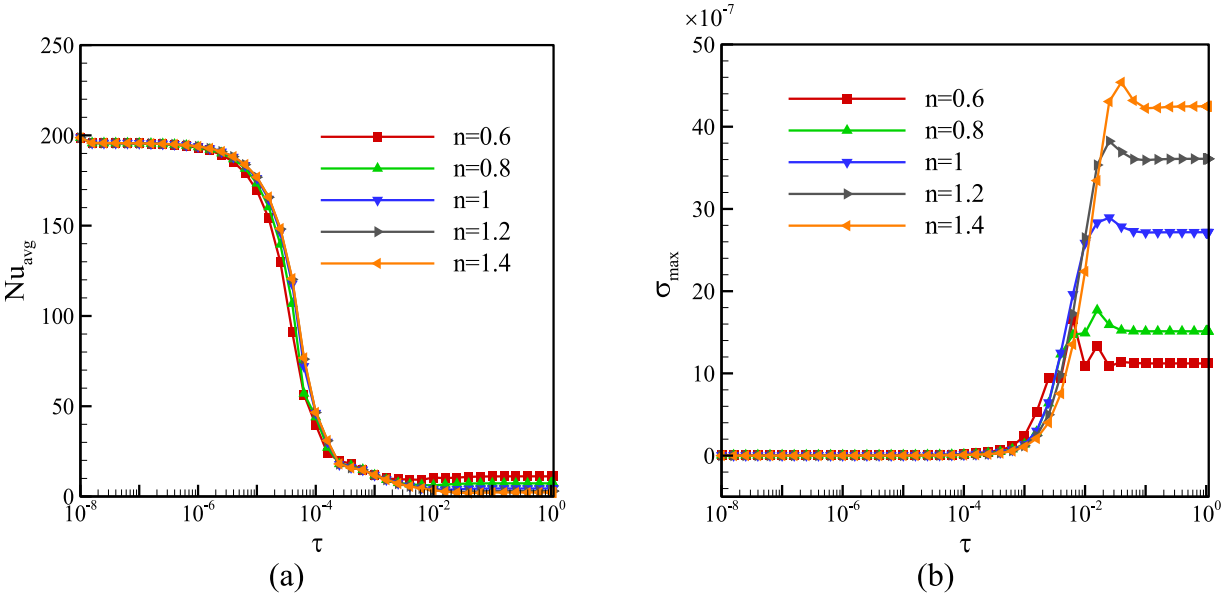

Fig. 9. The variations of (a): Nusselt number on the hot wall and (b): the maximum values of stress on the fin for different values of n at $Ra = 10^5$, $E_\tau = 10^{10}$, and $Pr = 10$.

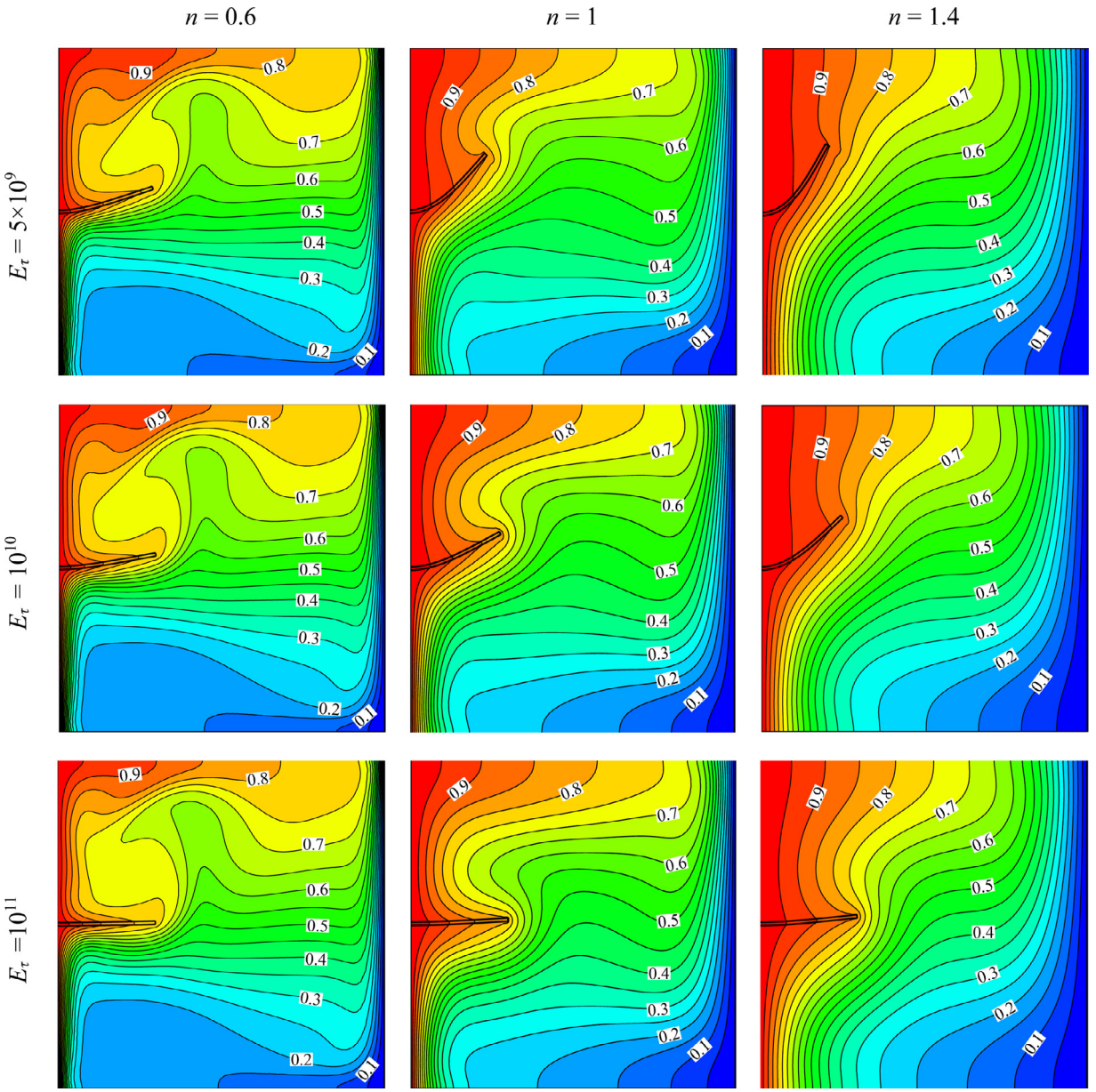

Fig. 10. The impact of the elasticity-modulus (flexibility) on the final patterns of the isotherms (steady-state) for various magnitudes of the power-law index (n = 0.6, 1, and 1.4) when $Ra = 10^5$, and $Pr = 10$.

For the pseudoplastic non-Newtonian fluid, i.e., $n < 1$, isotherms desire to stratify horizontally due to the effects of empowered natural convection. At a steady state situation, the jet of cold fluid forms along the cold wall and moves downward until it reaches the bottom wall. Then, it moves along the bottom wall. There is a jet of hot fluid over the hot wall, which tends to flow along the hot wall in an upward direction. However, when the jet reaches the flexible fin, the direction of jet changes along with the deflected position of the fin and leads to some circulation flows at the top-left corner. In pseudoplastic non-Newtonian power-low fluid (n = 0.6), the apparent fluid viscosity reduces by the higher stress. Hence, the presence of the fin induces significant alteration in flow patterns and isotherms.

For a dilatant fluid (n = 1.4), the apparent viscosity increases at high stresses, which occurs next to the structure boundaries. Thus, a higher degree of fluid-structure interaction can be anticipated for a dilatant fluid at a constant amount of buoyancy force. As a result, the amount of stress imposed on the fin for this fluid is more than Newtonian and pseudoplastic fluids, and therefore, a large fin deflection can be seen. Also, the pseudoplastic fluid acts as a damper of the buoyancy forces imposed on the fin; therefore, it leads to lower displacement of the fin compared with Newtonian and dilatant fluid.

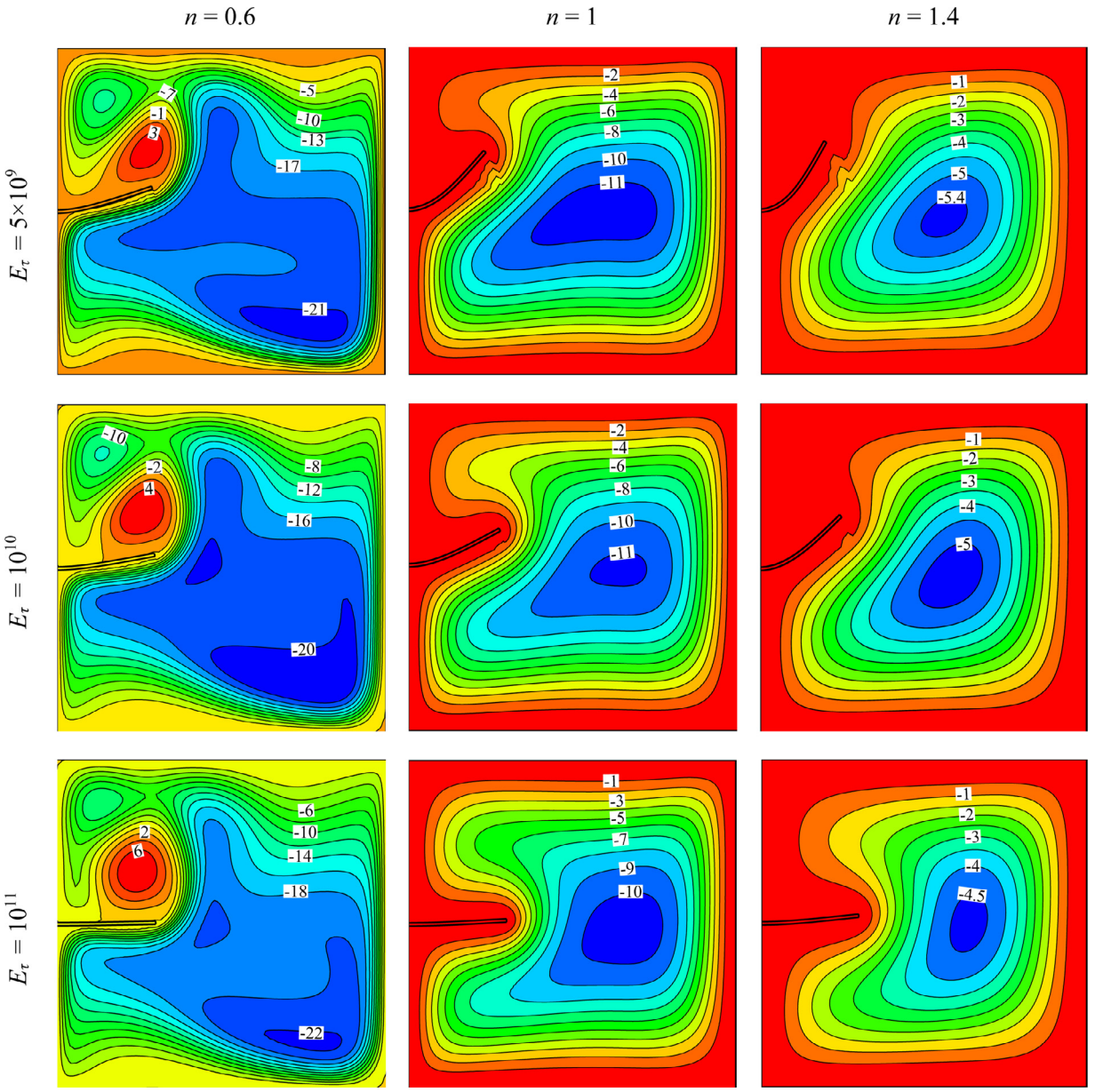

Fig. 11. The impact of the elasticity-modulus (flexibility) on the final patterns of the streamlines (steady-state) various magnitudes of the power-law index (n = 0.6, 1, and 1.4) when $Ra = 10^5$, and $Pr = 10$.

As seen in Fig. 8, at the primary time steps, four vortexes appear. There are two on the vertical hot wall, one at the tip of the fin and one next to the cold wall. Due to the leading role of the conduction mechanism in heat transfer and fluid circulation at this time, the vortices are weak. The vortices at the tip of the fin are disappeared at the next time snap ($\tau = 10^{-3}$), and the strength of core vortices at the center of the cavity increases. At all times, pseudoplastic accounts for the highest strength of the vortices compared with the Newtonian and dilatant fluids. It is the result of the lower rate of viscosity and resistance of this fluid in the face of buoyancy force, which leads to the most influence on this type of fluids. Therefore, although there are three counter-direction vortices for pseudoplastic fluids at the latest time snaps ($\tau = 10^{-2}$ and $\tau = 10^{\circ}$), one core vorticity can be seen for Newtonian and dilatant fluids.

Fig. 9 illustrates the effects of different values of n on the time variations of average Nusselt number on the hot wall and the maximum rate of stress produced in the fin at $Ra = 10^5$, $E_\tau = 10^{10,}$ and $Pr = 10$. As seen, various values of n have a slight impact on the average Nusselt number at the primary dimensionless time steps (10^{-8}–10^{-6}). This is because of the negligible natural convection in comparison with the conduction during these times for all types of investigated fluids, e.g., dilatant, Newtonian, and pseudoplastic fluids. At the following time-snaps (10^{-6}–10^{-3}), dilatant fluid demonstrates a higher

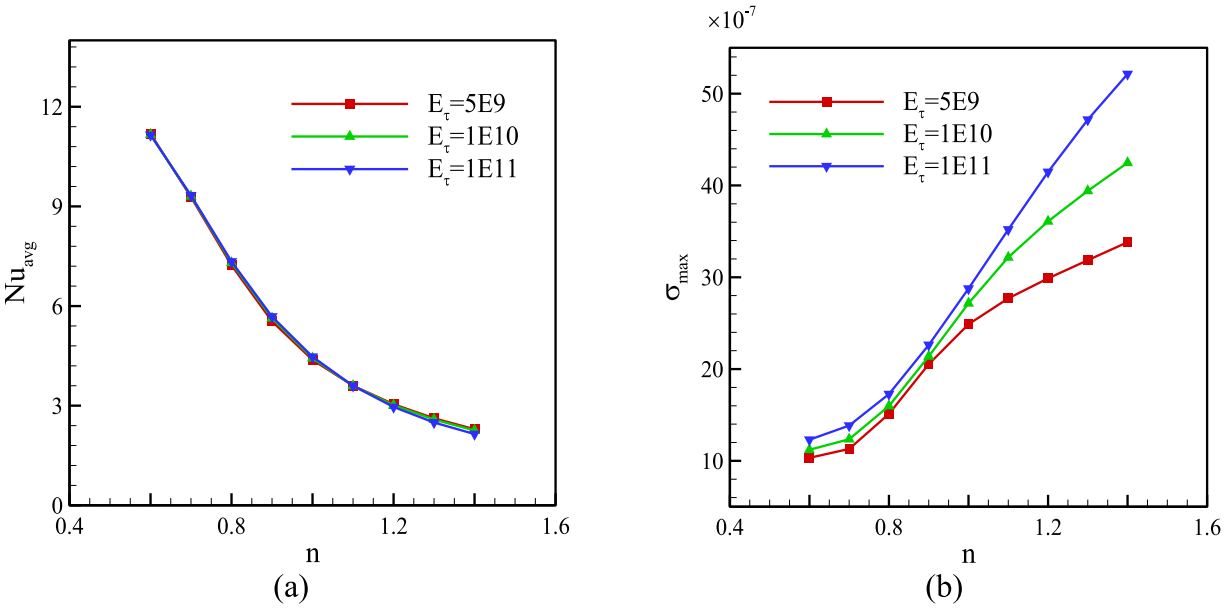

Fig. 12. The variations of (a) Nusselt number on the hot wall, and (b) the maximum values of stress on the fin for different values of n at different elasticity modules.

range of the average Nusselt number. At the final time duration (10^{-2}–10°), pseudoplastic fluids show higher values of the Nusselt number due to more flow rate and disturbance of this type of fluid inside the cavity for the same conditions leading to higher heat transfer rate.

All types of fluids experience an upward trend of maximum stress on the fin as time passes. As anticipated, the fin experiences the maximum stress at a higher range of n number. The viscosity of this fluid increases by the buoyancy force increment for ascending values of n; therefore, the imposed stress on fin increases. This trend can also be seen in Figs. 7 and 8, where the fin has the maximum displacement inside the fluid with $n = 1.4$.

Figs. 10 and 11 show the effects of elasticity modulus (E_τ) and different values of n on the isotherms and streamlines at a steady state. Higher E_τ causes higher resistance of the fin against the stress, so the displacement of the fin decreases as E_τ increases. Due to the resistance of a dilatant fluid against the buoyancy force, it hinders the advection mechanism, and the vertical isotherms pattern shows that the conduction is dominant for this fluid at the steady-state. According to Fig. 11, a triple-eye circulation for all elasticity modulus is depicted for pseudoplastic fluid. Three is a core vortex at the center, and there are two vortexes close to the fin tip and left the upper position of the vertical walls of the cavity. It is worth mentioning that the vortices close to the fin turn in the opposite direction compared with two other vortexes. The vortices close to the fin is weak because the fin inhibits the upward movement of flow induced by the natural convection. Also, the strength of vortices for pseudoplastic fluid is higher than Newtonian and dilatant fluid, respectively.

Fig. 12(a) and (b) presents the effects of average Nusselt number on the hot wall and the maximum stress on the fin for different values of n ($n = 0.6$–1.4) at three different elasticity modulus numbers. It can be seen that the Elasticity modulus does not affect the average Nusselt number. Higher n values lead to a decrease in the heat transfer rate. This is the reason for the low flow circulation of fluids with higher values of n. The maximum stress on the fin increases by growing n values. This is because the fluid with higher n accounts for the higher range of viscosity at constant shear, contributing to a higher force imposed on the fin. Also, the fin with higher elasticity modulus resists more against the fluid flow, so it shows a higher maximum-stress value.

Figs. 13 and 14 demonstrate the effects of Rayleigh number and different values of n on the isotherms and streamlines at steady-state for $E_\tau = 10^{10}$ and $Pr = 10$. There is no displacement of the fin at the lowest Rayleigh number ($Ra = 10^3$). Also, at this Rayleigh number, based on vertical stratification of the isotherms, conduction plays the leading role of the heat transfer. It is evident that higher Ra represents a higher buoyancy force. So, at $Ra = 10^4$, due to strengthened buoyancy force, there is higher flow movements and higher heat transfer rate. At this Rayleigh number, there is a small upward displacement of fin for $n = 1.4$. In the case of $n = 0.6$ and $Ra = 10^5$, the strengthened buoyancy forces notably disturb the domain located above the fin. The vortex patterns, including one core and two others above the fin, varies by the other streamlines comprising one core vortex.

Fig. 15(a) and (b) depicts the effects of average Nusselt number on the hot wall and the maximum stress in the fin for different values of n ($n = 0.6$–1.4) at three different Rayleigh numbers. As can be observed, a higher Rayleigh number

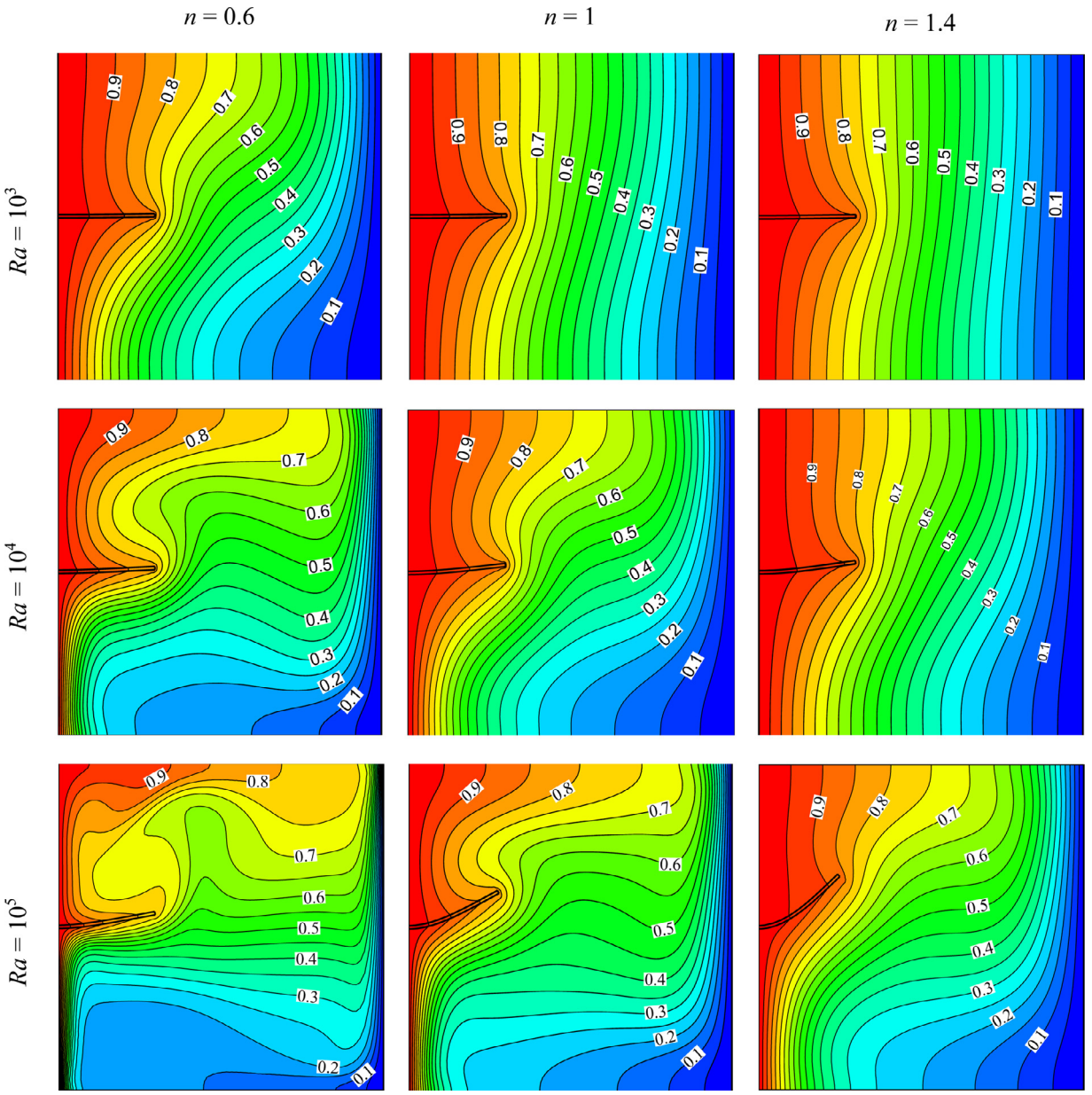

Fig. 13. The impact of Rayleigh number on the final patterns of the isotherms (steady-state) for various magnitudes of n (n = 0.6, 1, and 1.4) when $E_\tau = 10^{10}$, and $Pr = 10$.

demonstrates a higher heat transfer rate at a constant value of n. For lower values of n (n = 0.6–0.9), the average Nusselt number for $Ra = 10^4$ diagram is higher than its counterpart at higher ranges of n (n = 1.2, 1.3 and 1.4) for $Ra = 10^5$. Interestingly, the heat transfer for a low Rayleigh-number pseudoplastic-fluid (low values of n) is stronger that of a high Rayleigh-number dilatant-fluid (high values of n).

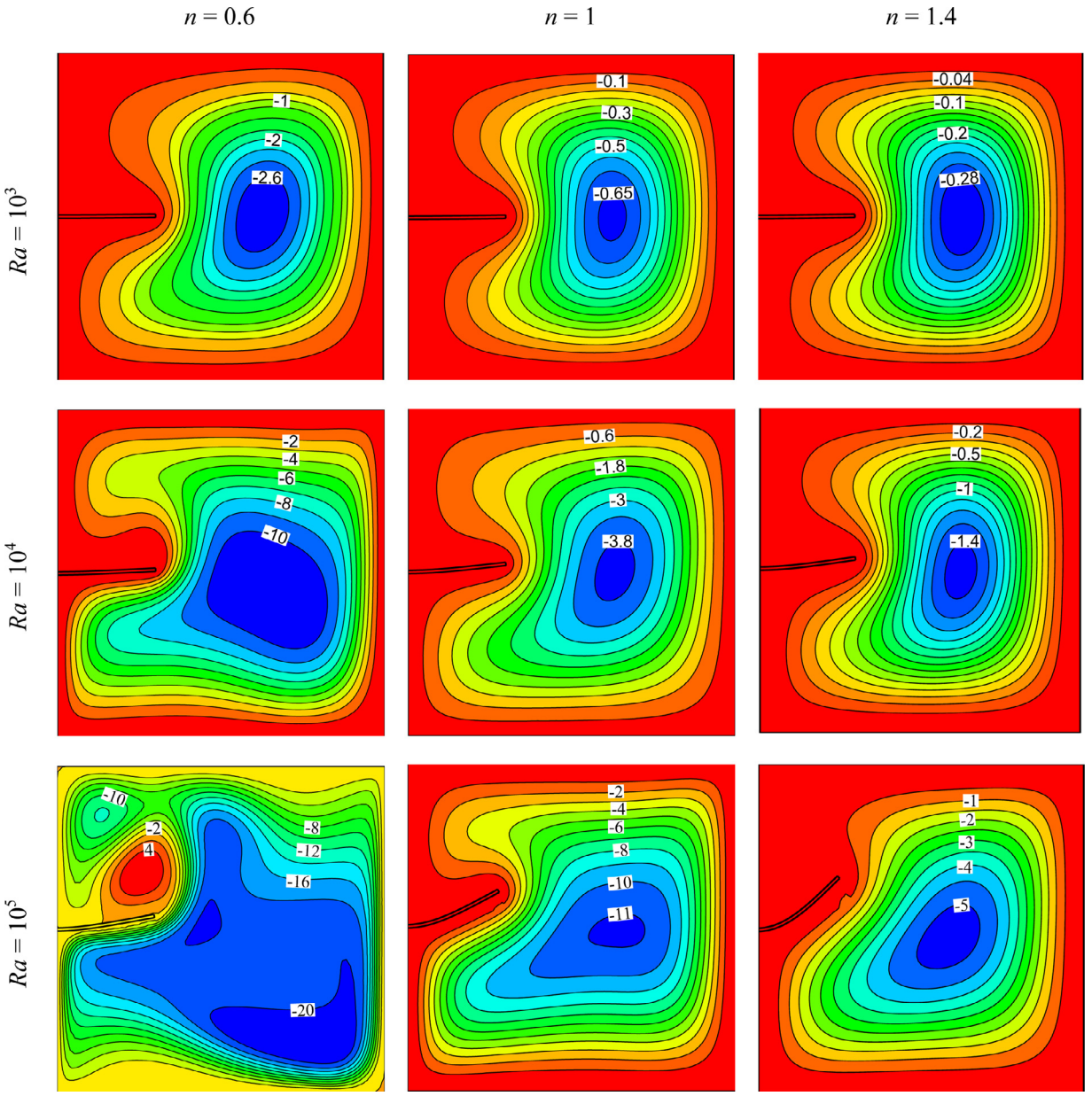

Fig. 14. The impact of Rayleigh number on the final patterns of the streamlines (steady-state) for various magnitudes of n (n = 0.6, 1, and 1.4) when $E_\tau = 10^{10}$, and $Pr = 10$.

All three diagrams show a downward trend in heat transfer by the increment of n. It is the result of a weakened flow rate for higher values of n. It can be seen that there is no stress on the fin at the lowest Rayleigh number ($Ra = 10^3$). For $Ra = 10^4$, an increase in n values leads to an increment of the maximum stress in the fin. For higher Rayleigh number ($Ra = 10^5$), the power index n shows noticeable role of elevating the strength of the buoyancy forces.

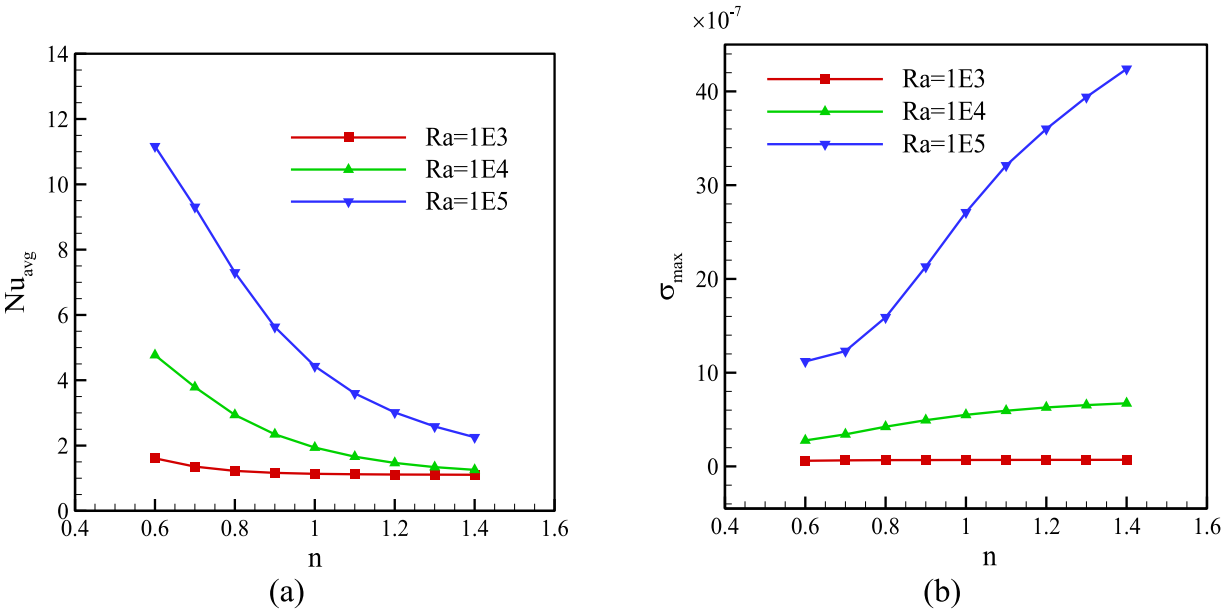

Fig. 15. The variations of a) Nusselt number on the hot wall, and b) the maximum values of stress on the fin for different values of n at three Rayleigh numbers.

5. Conclusion

In this paper, a numerical study was conducted to investigate the thermo-fluid characteristics and stress field of non-Newtonian power-law and Newtonian fluids inside a cavity equipped with a flexible fin. The left and right walls of the cavity are kept at the high and low isothermal temperatures of T_h and T_c, respectively, while the upper and lower walls were insulated. The deformation of the flexible fin was modeled by applying the fluid-structure interaction approach. The main results of this study are presented as follows:

- The main mechanism of heat transfer is conduction at the initial time steps, while the natural convection becomes dominant, gradually. The effects of buoyancy force on the vortices formed within the cavity is more significant for pseudoplastic fluid compared to a Newtonian fluid, due to lower resistance (viscosity) of this fluid against the stress. The higher viscosity of dilatant fluid compared with Newtonian and pseudoplastic fluid leads to more deflection of the fin.
- The hydrodynamic of the natural convection flow is under the significant influence of the non-Newtonian index and flexibility of the fin, particularly in the area above the fin.
- Various values of n do not affect the average Nusselt number on the hot wall at different time snaps considerably, while higher n value contributes to higher stress produced in the fin as time passes.
- The highest deformation of the fin is seen at the condition with a low elasticity modulus of the fin inside the dilatant fluid. Although the average Nusselt number on the hot wall is not affected by elasticity modulus, the stress is higher in the fin with higher elasticity modulus.
- All the results show downward and upward trends of heat transfer of the hot wall and stress in the fin by the increment in values of n, respectively.

References

[1] R.L. Webb, N. Kim, Enhanced Heat Transfer, Taylor and Francis, NY, 2005.
[2] N. Shashikumar, B. Gireesha, B. Mahanthesh, B. Prasannakumara, A.J. Chamkha, Entropy generation analysis of magneto-nanoliquids embedded with aluminium and titanium alloy nanoparticles in microchannel with partial slips and convective conditions, Int. J. Numer. Methods Heat Fluid Flow 29 (10) (2019) 3638–3658.
[3] M.S. Ishak, A.I. Alsabery, A. Chamkha, I. Hashim, Effect of finite wall thickness on entropy generation and natural convection in a nanofluid-filled partially heated square cavity, Int. J. Numer. Methods Heat Fluid Flow (2019).
[4] T. Tayebi, A.J. Chamkha, Entropy generation analysis during MHD natural convection flow of hybrid nanofluid in a square cavity containing a corrugated conducting block, Int. J. Numer. Methods Heat Fluid Flow (2019).
[5] M. Sheremet, T. Grosan, I. Pop, MHD free convection flow in an inclined square cavity filled with both nanofluids and gyrotactic microorganisms, Int. J. Numer. Methods Heat Fluid Flow 29 (2) (2019) 4642–4659.
[6] T. Groşan, M.A. Sheremet, I. Pop, S.R. Pop, Double-diffusive natural convection in a differentially heated wavy cavity under thermophoresis effect, J. Thermophys. Heat Transfer 32 (2018) 1045–1058.
[7] A.I. Alsabery, E. Gedik, A.J. Chamkha, I. Hashim, Impacts of heated rotating inner cylinder and two-phase nanofluid model on entropy generation and mixed convection in a square cavity, Heat Mass Transf. 56 (2020) 321–338.
[8] A. Alsabery, M. Sheremet, A. Chamkha, I. Hashim, Conjugate natural convection of Al_2O_3–water nanofluid in a square cavity with a concentric solid insert using Buongiorno's two-phase model, Int. J. Mech. Sci. 136 (2018) 200–219.

[9] A.I. Alsabery, R. Mohebbi, A.J. Chamkha, I. Hashim, Effect of local thermal non-equilibrium model on natural convection in a nanofluid-filled wavy-walled porous cavity containing inner solid cylinder, Chem. Eng. Sci. 201 (2019) 247–263.
[10] M.A. Ismael, Forced convection in partially compliant channel with two alternated baffles, Int. J. Heat Mass Transf. 142 (2019) 118455.
[11] M. Ghalambaz, E. Jamesahar, M.A. Ismael, A.J. Chamkha, Fluid-structure interaction study of natural convection heat transfer over a flexible oscillating fin in a square cavity, Int. J. Therm. Sci. 111 (2017) 256–273.
[12] E. Jamesahar, M. Sabour, M. Shahabadi, S. Mehryan, M. Ghalambaz, Mixed convection heat transfer by nanofluids in a cavity with two oscillating flexible fins: a fluid–structure interaction approach, Appl. Math. Model. 82 (2020) 72–90.
[13] M.A. Ismael, H.F. Jasim, Role of the fluid-structure interaction in mixed convection in a vented cavity, Int. J. Mech. Sci. 135 (2018) 190–202.
[14] A. Raisi, I. Arvin, A numerical study of the effect of fluid-structure interaction on transient natural convection in an air-filled square cavity, Int. J. Therm. Sci. 128 (2018) 1–14.
[15] U. Küttler, W.A. Wall, Fixed-point fluidstructure interaction solvers with dynamic relaxation, Comput. Mech. 43 (1) (2008) 61–72.
[16] F. Selimefendigil, H.F. Öztop, A.J. Chamkha, Fluid–structure-magnetic field interaction in a nanofluid filled lid-driven cavity with flexible side wall, Eur. J. Mech.-B/Fluids 61 (2017) 77–85.
[17] F. Selimefendigil, H.F. Öztop, Analysis of MHD mixed convection in a flexible walled and nanofluids filled lid-driven cavity with volumetric heat generation, Int. J. Mech. Sci. 118 (2016) 113–124.
[18] Y. Amini, H. Emdad, M. Farid, A. Chamkha, D. Wen, Fluid–structure interaction analysis of a piezoelectric flexible plate in a cavity filled with a fluid, Sci. Iran. 23 (2) (2016) 559–565.
[19] D.T. Yaseen, M.A. Ismael, Analysis of power law fluid-structure interaction in an open trapezoidal cavity, Int. J. Mech. Sci. 174 (2020) 105481.
[20] S. Ghelardi, C. Rizzo, D. Villa, Three-dimensional fluid-structure interaction case study on cubical fluid cavity with flexible bottom, J. Mar. Sci. Technol. 16 (4) (2017) 382–394.
[21] M. Chen, X. Niu, H. Yamaguchi, C. Shu, A lattice Boltzmann modeling fluid-structure interaction problems and its applications in natural convections in a square cavity with particles suspended inside, Adv. Appl. Math. Mech. 10 (2) (2018) 275–300.
[22] F. Irgens, Rheology and Non-Newtonian Fluids, Springer, 2014.
[23] M.H. Matin, I. Pop, S. Khanchezar, Natural convection of power-law fluid between two-square eccentric duct annuli, J. Non-Newton. Fluid Mech. 197 (2013) 11–23.
[24] A. Acrivos, M. Shah, E. Petersen, Momentum and heat transfer in laminar boundary-layer flows of non-Newtonian fluids past external surfaces, AIChE J. 6 (1960) 312–317.
[25] A.K. Dhiman, Heat transfer to power-law dilatant fluids in a channel with a built-in square cylinder, Int. J. Therm. Sci. 48 (2009) 1552–1563.
[26] A. Cavadas, F. Pinho, J. Campos, Laminar non-Newtonian impinging jet flow confined by sloping plane walls, J. Non-Newton. Fluid Mech. 169 (2012) 1–14.
[27] H. Ozoe, S.W. Churchill, Hydrodynamic stability and natural convection in Ostwald-de Waele and Ellis fluids: the development of a numerical solution, AIChE J. 18 (1972) 1196–1207.
[28] M. Ohta, M. Ohta, M. Akiyoshi, E. Obata, A numerical study on natural convective heat transfer of pseudoplastic fluids in a square cavity, Numer. Heat Transf.: Part A: Appl. 41 (2002) 357–372.
[29] L. Khezzar, D. Siginer, I. Vinogradov, Natural convection of power law fluids in inclined cavities, Int. J. Therm. Sci. 53 (2012) 8–17.
[30] Z. Alloui, P. Vasseur, Natural convection of Carreau–Yasuda non-Newtonian fluids in a vertical cavity heated from the sides, Int. J. Heat Mass Transf. 84 (2015) 912–924.
[31] F. Selimefendigil, A. Chamkha, MHD mixed convection in a lid-driven cavity having a corrugated bottom wall and filled with a non-Newtonian power-law fluid under the influence of an inclined magnetic field, J. Therm. Sci. Eng. Appl. 8 (2015) 1–8.
[32] A. Alsabery, A. Chamkha, H. Saleh, I. Hashim, Transient natural convective heat transfer in a trapezoidal cavity filled with non-Newtonian nanofluid with sinusoidal boundary conditions on both sidewalls, Powder Technol. 308 (2017) 214–234.
[33] Z. Raizah, A.M. Aly, S.E. Ahmed, Natural convection flow of a power-law non-Newtonian nanofluid in inclined open shallow cavities filled with porous media, Int. J. Mech. Sci. 140 (2018) 376–393.
[34] V. Anand, J. David Jr, I.C. Christov, Non-Newtonian fluid–structure interactions: static response of a microchannel due to internal flow of a power-law fluid, J. Non-Newton. Fluid Mech. 264 (2019) 62–72.
[35] Y. Qiao, Y. Zeng, Y. Ding, J. Fan, K. Luo, T. Zhu, Numerical simulation of two-phase non-Newtonian blood flow with fluid-structure interaction in aortic dissection, Comput. Methods Biomech. Biomed. Eng. 22 (2019) 620–630.
[36] W.A. Sabbar, M.A. Ismael, M. Almudhaffar, Fluid-structure interaction of mixed convection in a cavity-channel assembly of flexible wall, Int. J. Mech. Sci. 149 (2018) 73–83.
[37] J. Donea, A. Huerta, Finite Element Methods For Flow Problems, John Wiley & Sons, 2003.
[38] O.C. Zienkiewicz, R.L. Taylor, P. Nithiarasu, The finite element method for fluid dynamics, The Finite Element Method for Fluid Dynamics, Seven ed., utterworth-Heinemann, Oxford, 2014.
[39] F. Xu, J.C. Patterson, C. Lei, Heat transfer through coupled thermal boundary layers induced by a suddenly generated temperature difference, Int. J. Heat Mass Transf. 52 (2009) 4966–4975.
[40] B. Calcagni, F. Marsili, M. Paroncini, Natural convective heat transfer in square enclosures heated from below, Appl. Therm. Eng. 25 (2005) 2522–2531.
[41] M.H. Matin, W.A. Khan, Laminar natural convection of non-Newtonian power-law fluids between concentric circular cylinders, Int. Commun. Heat Mass Transf. 43 (2013) 112–121.